Electronic Journal of Biotechnology 83 (2026) 100708

Contents lists available at ScienceDirect

Electronic Journal of Biotechnology

journal homepage: www.elsevier.com/locate/ejbt

Research article

Analysis of drug resistance, virulence phenotype, and genetic sequences in microevolutionary strains of *Pseudomonas aeruginosa* MPAO1 ☆

Lingli Zhang [a], Huiping Qiu [a], Shuihong Yao [a], Pengxia Song [a], Zhenghui Li [b,*]

[a] Medical School, Quzhou College of Technology, Quzhou, PR China
[b] College of Chemical and Material Engineering, Quzhou University, Quzhou, PR China

GRAPHICAL ABSTRACT

Analysis of drug resistance, virulence phenotype, and genetic sequences in microevolutionary strains of *Pseudomonas aeruginosa* MPAO1.

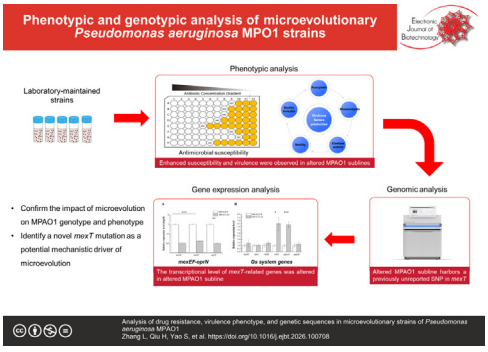

ARTICLE INFO

Article history:
Received 11 September 2025
Accepted 8 January 2026
Available online 9 February 2026

Keywords:
Antimicrobial susceptibility
Drug resistance
Efflux pump regulation
MexEF-OprN efflux pump
mexT mutation
Microevolution
Pseudomonas aeruginosa MPAO1
Quorum sensing
Virulence factors

ABSTRACT

Background: The *Pseudomonas aeruginosa* PAO1 strain is a foundation of research on bacterial virulence and antibiotic resistance. However, its tendency for microevolution during laboratory culture can lead to genetic and phenotypic divergence, potentially compromising experimental reproducibility. This study aimed to systematically characterize such variations in laboratory-maintained MPAO1 sublines to assess their genetic stability and suitability for research.

Results: We identified two distinct MPAO1 sublines (MPAO1-P and MPAO1-M) with divergent phenotypes. MPAO1-M exhibited markedly increased antimicrobial susceptibility to multiple antibiotics, including ciprofloxacin, imipenem, gentamicin and chloramphenicol, while concurrently displaying enhanced production of key virulence factors, including pyocyanin, rhamnolipids, elastase, and twitching motility. Whole-genome resequencing uncovered a novel missense mutation in the mexT gene of MPAO1-M. Consistent with this finding, quantitative reverse transcription PCR analysis revealed a significant downregulation of the mexEF-oprN efflux pump operon and a marked upregulation of the quorum-sensing genes rhlI and pqsA.

Conclusions: Our findings confirm the critical impact of microevolution on MPAO1 genotype and phenotype, underscoring the necessity of strain verification in experimental design. We further identify a novel mexT mutation as a potential mechanistic driver of these changes, providing new insights into the

☆ Audio abstract available in Supplementary material.

* Corresponding author.
E-mail address: zhenghuilz@outlook.com (Z. Li).

https://doi.org/10.1016/j.ejbt.2026.100708

genetic basis of adaptive evolution in laboratory P. aeruginosa strains.

How to cite: Zhang L, Qiu H, Yao S, et al. Analysis of drug resistance, virulence phenotype, and genetic sequences in microevolutionary strains of *Pseudomonas aeruginosa* MPAO1. Electron J Biotechnol 2026;82. https://doi.org/10.1016/j.ejbt.2026.100708.

1. Introduction

Pseudomonas aeruginosa, a Gram-negative opportunistic pathogen, represents a formidable clinical challenge owing to its pivotal role in life-threatening systemic infections. This pathogen's intricate virulence regulatory networks, coupled with its remarkable antimicrobial resistance capacity, have driven its increasing prevalence in healthcare-associated infections, significantly contributing to elevated morbidity and mortality rates in clinical settings [1].

P. aeruginosa produces diverse virulence factors that enable environmental adaptation and host invasion. Pyocyanin induces oxidative stress via reactive oxygen species generation by disrupting membranes and cellular processes [2]. Elastase degrades immunoglobulins and complement proteins while destroying host tissues, exacerbating infections [3]. Type IV pili and flagella mediate motility (twitching/swimming/swarming), promoting biofilm formation [4]. Biofilms represent matrix-encased microbial communities that resist antibiotics and immune clearance through coordinated defenses [5]. Rhamnolipids regulate biofilm maturation and structural integrity during later stages [6]. Clinical infection severity directly correlates with virulence factor activity, explaining P. aeruginosa's capacity to cause acute and chronic disease.

The production of virulence factors and biofilm development in *P. aeruginosa* are tightly coordinated by a sophisticated quorum-sensing (QS) mechanism, which functions as a density-responsive intercellular signaling network. This system consists of several well-defined signaling pathways, including the extensively characterized Las, Rhl and PQS systems [7,8]. Additionally, environmental cues such as phosphate limitation can modulate virulence factor production through complex interactions with the QS network, although the exact regulatory mechanisms, including the previously proposed but controversial IQS system, require further clarification [8,9]. The Las system is mediated by the *lasI*-dependent synthesis of the autoinducer 3-oxo-C12-HSL (N-3-oxododecanoyl-L-homoserine lactone), which activates the transcriptional regulator LasR. The Rhl system involves *rhlI*-encoded production of C4-HSL (N-butyryl-L-homoserine lactone), detected by the response regulator RhlR. The PQS system is governed by the *pqsABCDE* operon, generating the *Pseudomonas* quinolone signal, which binds the transcriptional activator PqsR (also called MvfR). Upon reaching threshold concentrations, these signaling molecules initiate a hierarchical regulatory cascade, ultimately modulating the expression of QS-dependent genes, including those involved in the production of virulence factors and biofilm formation [10].

P. aeruginosa exhibits multifaceted antimicrobial resistance mechanisms, involving mutations in drug target genes, biosynthesis of antibiotic-modifying enzymes, dysregulation of efflux pump systems, reduced outer membrane permeability, and formation of protective biofilms [11,12]. The resistance-nodulation-division (RND) family efflux pumps, particularly MexAB-OprM, MexCD-OprJ, MexXY-OprM and MexEF-OprN, constitute critical determinants of *P. aeruginosa* resistance by actively expelling various antimicrobial agents [13]. Genomic alterations in genes encoding transcriptional regulators frequently compromise negative feedback loops controlling efflux pump expression, leading to their sustained overexpression. For example, mutations in *mexR*, *nalC*, and *nalD* genes derepress *mexAB-oprM* expression [14,15,16]. *mexT* mutations result in *mexEF-oprN* overexpression [17]. This dysregulated overexpression of key RND efflux systems is a major mechanism driving decreased susceptibility to clinically important antimicrobial classes, including aztreonam, carbapenems, fluoroquinolones and chloramphenicol [14,16,17].

The reference strain PAO1 of *P. aeruginosa* is widely employed in the study of pathogenicity and antimicrobial resistance mechanisms. However, its utility is compromised by a well-documented propensity for microevolution during laboratory maintenance, which can lead to significant genomic and phenotypic divergence between sublines [18]. Notable examples include PAO1-UW, which harbors a 2.2 Mb chromosomal inversion, and PAO1-DSM, which carries loss-of-function mutations in mexT and lasR that alter antibiotic susceptibility and virulence [19,20,21]. These strain-specific phenotypes profoundly impact experimental outcomes, reinforcing the necessity of subline verification.

Consistent with this trend, our laboratory observed unexplained discrepancies in the antimicrobial susceptibility profiles of contemporary MPAO1 cultures compared to archival records. This study originated from investigating these deviations to determine whether they reflected stochastic fluctuations or a systematic microevolutionary event. We conducted a comprehensive phenotypic and genomic comparison between the original MPAO1 stock and its propagated derivatives. Our integrated approach, combining whole-genome resequencing (WGRS) with phenotypic assays and transcriptional profiling, aimed not only to identify the genetic basis of the divergence but also to serve as a case study highlighting the critical impact of strain integrity on experimental reproducibility.

2. Materials and methods

2.1. Bacterial strains and growth conditions

The MPAO1 original strain MPAO1-19 was commercially obtained from Guangzhou Maibo Bioscience Co., Ltd. in 2019 and has been preserved in our laboratory at −80°C in glycerol stock as Passage 0. Its complete genomic characteristics are presented in Table 1. The strains of *P. aeruginosa* MPAO1 examined in this research were derived from this common ancestor MPAO1-19 through two independent propagation lines. For the MPAO1-P subline, MPAO1-19 was subjected to serial passage in Luria-Bertani (LB) broth. After five passages, single colonies were isolated from the culture to generate the biologically independent strains MPAO1-20, MPAO1-21, and MPAO1-22. The MPAO1-M subline strains (MPAO1-23A and MPAO1-23B) were isolated as single colonies from a separate, independent serial passage series of MPAO1-19 that was maintained over a longer duration, during which the evolved phenotype emerged. The *P. aeruginosa* MPAO1 strains were cultivated in LB medium under 37°C condition.

Table 1
Genome characteristics of MPAO1.

Strain	Sequence ID	NCBI BioSample Accession No.	Genome size (bp)	GC content (%)
MPAO1	CP027857.1	SAMN08722738	6,275,467	66.54

2.2. Determination of antimicrobial susceptibility

Susceptibility test was conducted following Kirby-Bauer (K-B) method. The disk diffusion assays were performed under the following standardized conditions: on Mueller-Hinton agar plates with a depth of 4 mm, using antibiotic discs from a single batch for each experiment, and with all plates incubated under identical environmental conditions without stacking. The following antibiotic disks (Solarbio, China) were tested: ciprofloxacin (5 μg), ceftazidime (30 μg), aztreonam (30 μg), imipenem (10 μg), gentamicin (10 μg) and chloramphenicol (30 μg). These antibiotics were chosen based on their clinical applicability. After an 18 h-incubation at 37°C, the diameters of the inhibition zones were recorded. All conditions were evaluated in biological replicates ($n \geq 4$), and the results are reported as mean ± standard deviation (SD).

The minimal inhibitory concentrations (MICs) of ciprofloxacin, gentamicin, imipenem and chloramphenicol were determined by the broth microdilution method [22]. All conditions were tested in biological replicates (n = 3), and the results are reported as mean ± SD. The breakpoints used for interpretation were those recommended by the Clinical and Laboratory Standards Institute (CLSI) M100, 35th Edition (M100-Ed35), published in 2025.

2.3. Growth curve measurement

Overnight cultures of the MPAO1 strains were diluted to an OD_{600} of 0.1 in LB broth. A total of 200 μL aliquots of each suspension were dispensed in technical triplicate into a 96-well plate and incubated at 37°C in a microplate reader (SpectraMax iD3) with continuous shaking (200 rpm) for 24 h. OD_{600} was recorded automatically every hour [23]. Blank-corrected data were used to generate growth curves, which were analyzed as mean ± SD (n = 3 biological replicates).

2.4. Pyocyanin quantification

To quantify pyocyanin production, MPAO1 strains were cultured in 50 mL LB medium under 37°C with 200 rpm agitation for 48 h. Cell density was determined by measuring OD_{600}. After centrifugation (7000 × g, 10 min) of 3 mL culture to pellet bacterial cells, the pyocyanin-containing supernatant was processed by chloroform extraction (1:1 v/v), followed by back-extraction into 0.2 M HCl (1 mL) [23]. Pyocyanin concentration was determined spectroscopically at 520 nm (A_{520}). Yields were normalized to volume and expressed as A_{520}/mL. The biological replicates (n = 3) were performed, with data presented as mean ± SD.

2.5. Rhamnolipid detection

To assess rhamnolipid production, three biologically independent replicates (n = 3) of overnight LB cultures were prepared for each MPAO1 strain. For each biological replicate, 10 μL aliquots were plated in technical triplicate on solid M9 minimal medium plates supplemented with glutamate (0.5% w/v), cetyltrimethylammonium bromide (CTAB, 0.2 g/L), and methylene blue (0.005 g/L). Following 48 h at 37°C, both halo diameter (HD) and colony diameter (CD) were measured as indicators of rhamnolipid secretion and growth, respectively [23]. Rhamnolipid activity was quantified as HD minus CD, and the results were presented as mean ± SD.

2.6. Elastase activity determination

Overnight LB-grown cultures of MPAO1 strains were centrifuged, and elastin Congo Red assays were initiated by adding 100 μL of centrifuged supernatant to the solution composed of 0.1 M Tris-HCL and 10 g/L elastin Congo Red. The reaction mixtures were incubated for 18 h at 37°C, followed by centrifugation and measurement of supernatant absorbance at 495 nm (A_{495}) [23]. Results were normalized to cell density (determined by OD_{600} of pre-centrifuged cultures), expressed as A_{495}/OD_{600}. The biological replicates (n = 3) per strain were performed, with data reported as mean ± SD.

2.7. Motility assay

2.7.1. Swarming

Prior to inoculation, all swarm plates composed of dextrose (5 g/L), nutrient broth (8 g/L) and agar (0.5%) were dried uncovered in a laminar flow hood for 30 min to achieve a dry surface. Two μL from overnight LB-grown cultures were spotted on swarm plates and incubated at 37°C for 24 h. The extent of swarming was assessed through diameter measurements of the spreading bacterial cloud originating from the inoculation site [21]. This assay was carried out in biological replicates (n = 3) and reported as mean ± SD.

2.7.2. Swimming

Overnight LB broth cultures were inoculated as 2 μL aliquots onto swim plates (NaCl 0.5%, tryptone 1%, agar 0.3%). Following 24 h incubation at 37°C, motility was quantified by measuring radial expansion from the inoculation site [21]. This assay was carried out in biological replicates (n = 3).

2.7.3. Twitching

Microbial cultures were inoculated vertically into LB agar (1% w/v) using sterile toothpicks, penetrating to the base of the culture plates. Following 24-h incubation at 37°C, the solid medium was carefully removed. Non-adherent cells were eliminated by thorough washing with water under a gentle stream, and biofilm formation was subsequently visualized by staining with 1% (w/v) crystal violet solution [21]. This assay was carried out in biological replicates (n = 3).

All motility plates were incubated in a humidified chamber to prevent desiccation during the experiment.

2.8. Biofilm formation analysis

Biofilm formation ability was determined using the crystal violet assay. Overnight cultures of each MPAO1 strain were diluted to OD_{600} = 0.1 and grown at 37°C in a 96-well plate containing LB broth. After incubation for 24 h and 48 h, planktonic cells were eliminated through three sequential washes using phosphate-buffered saline (PBS, pH 7.4). The remaining biofilm matrices were immobilized by incubation with 4% formaldehyde for 10 min, followed by staining with a 0.1% (w/v) aqueous crystal violet solution for 30 min, unbound dye and loosely attached cells were then com-

pletely removed by extensive rinsing with distilled water under gentle agitation. Biofilm-incorporated dye was subsequently extracted with 200 μL of absolute ethanol (95%). Biofilm biomass was determined by measuring OD_{590} of the ethanol-dissolved crystal violet. This assay was carried out in biological replicates (n = 6) and reported as mean ± SD.

2.9. Genomic DNA extraction and whole-genome resequencing

Genomic DNA was extracted from bacterial cells and subjected to WGRS (Shanghai Personal Biotechnology Co., Ltd). Libraries were constructed following the manufacturer's protocol for Illumina TruSeq Nano DNA LT library preparation. The libraries were evaluated for integrity using the Agilent Bioanalyzer 2100 system with the High Sensitivity DNA analysis kit and quantified via PicoGreen dsDNA assay (minimum concentration: 2 nM). High-throughput paired-end sequencing (150 bp × 2) was conducted using an Illumina NovaSeq platform. Quality control was carried out with FastQC (V0.12.1) to obtain high-throughput raw data. Short reads were mapped to the *P. aeruginosa* MPAO1 reference genome CP027857.1 (NCBI accession number SAMN08722738) using BWA-MEM v0.7.17.

WGRS information for the analyzed strains is presented in Table 2. The raw WGRS data have been deposited at NCBI with the following accessions: strain MPAO1-21 is available under BioProject PRJNA1309694, BioSample SAMN50750974, and SRA Run SRR35093329; while strain MPAO-23B is accessible through BioProject PRJNA1309779, BioSample SAMN50758596, and SRA Run SRR35102198.

2.10. Genetic variant detection and annotation

Single-nucleotide polymorphisms (SNPs) and insertion-deletion variants (InDels) were detected using the Genome Analysis Toolkit (GATK, v4.2.4.0). SNPs were called under stringent quality filters: Fisher's Strand Bias Test (FS) ≤ 60, Haplotype Score (HaplotypeScore) ≤ 13.0, Mapping Quality (MQ) ≥ 40, Quality by Depth (QD) ≥ 2, Read Position Rank Sum Test (ReadPosRankSum) ≥ −8.0, Mapping Quality Rank Sum Test (MQRankSum) > −12.5, Minimum alternative allele depth (AD) ≥ 4 reads. InDels were identified using GATK's UnifiedGenotyper and SelectVariants, applying the same quality thresholds as for SNPs. Genome-wide copy number variations (CNVs) were identified using CNVnator (bin size = 100 bp), excluding natural multicopy regions. Read-depth (RD) thresholds were established relative to a diploid baseline (RD = 1): deletions were defined as RD ≤ 0.05, and amplifications as RD ≥ 1.8. All identified variants (SNPs, InDels and CNVs) were annotated to predict functional impacts using ANNOVAR.

2.11. Quantitative reverse transcription PCR

Overnight LB-grown cultures of MPAO1 sublines were incubated at 37°C for 24 h. RNA was extracted using the EZ-10 Spin Column Total RNA Isolation Kit. Following quality control verification (NanoDrop ND-1000; 260/280 nm ratios: 1.8–2.2), cDNA synthesis was performed with TransScript First-Strand cDNA Synthesis SuperMix using 1 μg RNA input as specified by the manufacturer. Quantitative PCR was carried out in 20 μL reactions using PerfectStart Green qPCR SuperMix on a Bio-Rad CFX96 system. The thermal protocol included an initial step of 95°C, 30 s, followed by 40 cycles of 95°C, 5 s, 57°C, 15 s and 72°C, 10 s. No-template controls with nuclease-free water replacing cDNA and negative control samples without reverse transcriptase were included. Expression levels were calculated via the $2^{-\Delta\Delta CT}$ method, with *rpsL* as the endogenous control. These experiments were carried out in biological replicates (n = 3), and the results were expressed as mean ± SD. Primers are listed in Table 3.

2.12. Statistical analysis

All quantitative data are presented as means ± SD from at least three independent biological replicates. Statistical analysis was performed using SPSS software (version 21.0). The data underwent

Table 2
Summary of sequencing and mapping statistics for all samples.

Sample	Raw reads	HQ reads	Q30 (%)	Mapping rate (%)	Coverage (≥20×) (%)	Depth (X)
MPAO1-21	7,807,03	7,487,666	94.98	99.90	100	179
MPAO1-23B	9,297,158	8,883,844	94.79	99.88	100	212

Table 3
Primers used in this study.

Primers	Sequences (5′→3′)	Amplicon sizes	Amplification efficiency	Source or references
lasR-F	CAAGTGGAAAATTGGAGTGGAG	132 bp	101.8%	This study
lasR-R	GGGTAGTTGCCGACGATGAA			This study
lasI-F	TGCGTGCTCAAGTGTTCAAGG	246 bp	101.6%	This study
lasI-R	CGGCTGAGTTCCCAGATGTGC			This study
rhlR-F	CTCCTCGGAAATGGTGGTCT	138 bp	104.3%	This study
rhlR-R	GAAAGCACGCTGAGCAAATT			This study
rhlI-F	GAAGATATTCTGGTCCAGCCTG	147 bp	105.3%	This study
rhlI-R	TCGCCCTTGACCTTCTGC			This study
pqsR-F	TCGTTCTGCGATACGGTGAG	167 bp	104.1%	This study
pqsR-R	GCACTGGTTGAAGCGGGAG			This study
pqsA-F	GCAATACACCTCGGGTTCCA	189 bp	101.4%	This study
pqsA-R	TCCGCTGAACCAGGGAAAGA			This study
mexE-F	CCGGATCGTCGTGAATGGC	138 bp	104.5%	This study
mexE-R	CTTCGGTGGTTCGCTGTCG			This study
mexF-F	CGCCTGGTCACCGAGGAAGAGT	254 bp	102.3%	[24]
mexF-R	TAGTCCATGGCTTGCGGGAAGC			[24]
oprN-F	GCAACCTGGAGAACCAGAAGGA	213 bp	104.0%	This study
oprN-R	GGCGAAAGGTCCACTGTCAACT			This study
rpsL-F	CGGCACTGCGTAAGGTATGC	212 bp	101%	[25]
rpsL-R	CGTACTTCGAACGACCCTGCT			[25]

assessment of normality and homogeneity of variance. When distributions satisfied both normality and homogeneity of variance requirements, comparisons were conducted using either the independent-samples *t*-test (for two groups) or one-way ANOVA (for ≥3 groups), followed by Tukey's post-hoc test. For datasets failing these assumptions, nonparametric methods were employed: the Mann-Whitney test (two-group comparisons) and Kruskal-Wallis test (multi-group comparisons). Statistical significance was defined at $p < 0.05$.

3. Results

3.1. Antimicrobial susceptibility of MPAO1 strains

To assess variations in antimicrobial susceptibility among laboratory-maintained MPAO1 strains, we initially employed the K-B method to evaluate susceptibility profiles against clinically relevant anti-*Pseudomonas* antibiotics, including ciprofloxacin, ceftazidime, aztreonam, imipenem and gentamicin. Although not recommended for clinical testing against *P. aeruginosa*, chloramphenicol was also included based on previous studies [26], which reported altered susceptibility in certain *P. aeruginosa* variants. Its inclusion allowed us to directly benchmark our results against established data and provided an internal control for assessing the functionality of the mechanism under investigation.

Two distinct phenotypic groups were identified in this antimicrobial susceptibility analysis (Table 4). Strains MPAO1-19, -20, -21, and -22 exhibited homogeneous susceptibility profiles with no significant differences in inhibition zone diameters for any antibiotic tested (ciprofloxacin: $p = 0.998$; ceftazidime: $p = 1.000$; aztreonam: $p = 0.914$; imipenem: $p = 0.715$; gentamicin: $p = 0.806$; chloramphenicol: $p = 0.897$). Similarly, MPAO1-23A and -23B displayed equivalent antibiotic susceptibility (ciprofloxacin: $p = 0.985$; ceftazidime: $p = 0.854$; aztreonam: $p = 0.980$; imipenem: $p = 0.961$; gentamicin: $p = 0.803$). Based on the observed patterns of susceptibility, we classified the strains maintaining the ancestral susceptibility pattern as the MPAO1-P subline, and those showing altered susceptibility (MPAO1-23A and MPAO1-23B) as the MPAO1-M subline. Notably, while both sublines showed comparable susceptibility to ceftazidime ($p = 0.484$) and aztreonam ($p = 0.198$), MPAO1-M exhibited significantly larger inhibition zones than MPAO1-P for ciprofloxacin, imipenem, gentamicin, and chloramphenicol (all $p < 0.001$), indicating substantially enhanced susceptibility to these antimicrobial agents.

To confirm the differential susceptibility patterns identified by K-B assays between MPAO1-P and MPAO1-M sublines, MIC determinations were performed for critical antibiotics demonstrating K-B phenotype divergence. Results in Table 5 showed that ciprofloxacin MIC decreased ≥8-fold in MPAO1-M ($p < 0.001$), confirming its differential K-B zone pattern; imipenem, chloramphenicol showed (2–4)-fold and gentamicin showed 2-fold MIC reductions in MPAO1-M ($p < 0.05$), aligning with K-B results. These MIC data validate the MPAO1-P/MPAO1-M dichotomy and suggest the emergence of distinct genomic or epigenomic alterations that drive the divergent resistance profiles between sublines.

Table 5
MICs of antibiotics to MPAO1 sublines.

Antibiotics	MIC range (mg/L)		Fold change
	MPAO1-P	MPAO1-M	
CIP	1 [S]	<0.125–0.125 [S]	≥ 8
IMP	4 [I]	1–2 [S]	2–4
GEN	4	2	2
CHL	256–512	128	2–4

CIP: Ciprofloxacin; IMP: Imipenem; GEN: Gentamicin; CHL: Chloramphenicol; S: Susceptible; I: Intermediate. Breakpoints for gentamicin have been discontinued in the CLSI (M100-Ed35, 2025), and no breakpoints are established for chloramphenicol against *P. aeruginosa*. Experiments were carried out in biological replicates ($n = 3$).

3.2. Growth kinetics of MPAO1 strains

The growth dynamics of MPAO1 sublines were monitored over a 24-h period in LB broth (Fig. 1). Both sublines exhibited classic bacterial growth curves, progressing through lag, exponential, and stationary phases. Quantitative analysis revealed no significant differences in growth kinetics between the ancestral MPAO1-P group (strains MPAO1-19, -20, -21, -22) and the evolved MPAO1-

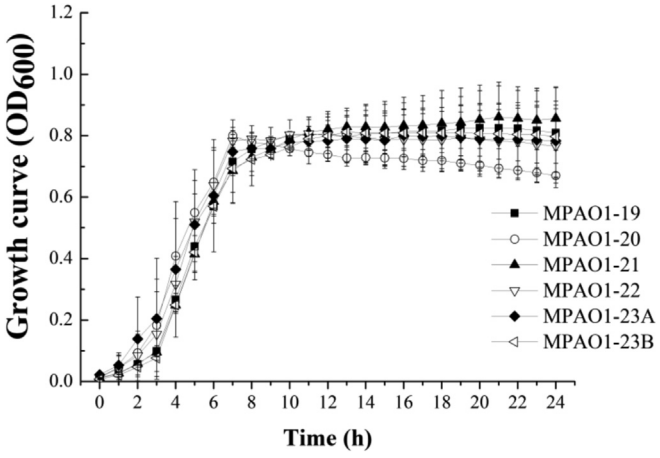

Fig. 1. Growth curves of MPAO1 sublines over a 24 h period in LB broth. Values represent mean OD_{600} ± SD of the biological replicates ($n = 3$) per strain. No significant inter-strain differences at any timepoint (one-way ANOVA, $p > 0.05$).

Table 4
Susceptibility of *P. aeruginosa* MPAO1 strains to antibiotics.

Antibiotics	Inhibition zone diameter (mm)					
	MPAO1-P				MPAO1-M	
	MPAO1-19	MPAO1-20	MPAO1-21	MPAO1-22	MPAO1-23A	MPAO1-23B
CIP	31.86 ± 4.67[a] (S)	31.87 ± 4.88[a] (S)	32.29 ± 4.94[a] (S)	32.11 ± 5.36[a] (S)	40.14 ± 6.84[b] (S)	40.07 ± 7.49[b] (S)
CAZ	28.71 ± 3.85[a] (S)	28.79 ± 4.06[a] (S)	28.57 ± 3.83[a] (S)	28.71 ± 4.09[a] (S)	29.57 ± 4.53[a] (S)	30.14 ± 6.68[a] (S)
ATM	28.17 ± 2.69[a] (S)	27.83 ± 2.65[a] (S)	28.03 ± 2.77[a] (S)	28.09 ± 2.54[a] (S)	29.51 ± 4.24[a] (S)	29.29 ± 4.68[a] (S)
IMP	14.5 ± 3.00[a] (R)	15.38 ± 3.04[a] (R)	14.38 ± 2.81[a] (R)	14.5 ± 2.92[a] (R)	19.63 ± 1.93[b] (S)	20.25 ± 2.63[b] (S)
GEN	22.50 ± 0.58[a]	22.36 ± 0.48[a]	22.83 ± 1.09[a]	22.75 ± 0.65[a]	31.75 ± 2.90[b]	31.25 ± 2.50[b]
CHL	0[a]	0[a]	0[a]	0[a]	20.86 ± 1.18[b]	21.00 ± 1.41[b]

CIP: Ciprofloxacin; CAZ: Ceftazidime; ATM: Aztreonam; IMP: Imipenem; GEN: Gentamicin; CHL: Chloramphenicol. Data were reported as mean ± SD of biological replicates (n ≥ 4). Superscript letters (a, b) indicate significant differences within rows ($p < 0.05$). Values sharing the same letter do not differ significantly ($p > 0.05$). (S): Susceptible; (R): Resistant. Breakpoints for gentamicin have been discontinued in the CLSI (M100-Ed35, 2025), and no breakpoints are established for chloramphenicol against *P. aeruginosa*.

M group (strains MPAO1-23A, -23B) ($p > 0.05$). These results confirm that phenotypic divergence in antibiotic resistance between sublines is independent of growth rate or biomass accumulation under standard laboratory conditions.

3.3. Production of virulence factors in MPAO1 strains

To further characterize the pathogenic divergence between the MPAO1-P and MPAO1-M sublines, we quantified key virulence factors across the MPAO1 strains, including pyocyanin, rhamnolipid, elastase production, motility and biofilm formation.

3.3.1. Pyocyanin

Pyocyanin production was tested by measuring the OD_{520} of the pyocyanin pigment produced by MPAO1 strains. As a result, the pyocyanin production levels revealed negligible differences ($p = 0.448$) among strains MPAO1-19, MPAO1-20, MPAO1-21, and MPAO1-22, which were all significantly lower (mean 24.8-fold, $p < 0.001$) than those of MPAO1-23A and MPAO1-23B (Fig. 2).

3.3.2. Rhamnolipid

Rhamnolipid forms insoluble CTAB complexes in solid media, producing dark blue halos upon methylene blue staining. This halo formation provides a semi-quantitative measure of rhamnolipid production; the colony size served as growth control. The result demonstrated that both MPAO1-23A and -23B exhibited a significantly 3.53-fold larger halo than the other strains ($p < 0.001$, Fig. 3), confirming enhanced rhamnolipid biosynthesis in these variants. Despite comparable growth kinetics in liquid LB medium (Fig. 1), the significantly reduced colony size observed for MPAO1-23A/B ($p = 0.007$) on solid CTAB-methylene blue plates suggests distinct spatial adaptation associated with altered resource allocation, likely concomitant with elevated secondary metabolite production in this subline.

3.3.3. Elastase

Elastase activity of MPAO1 strains was determined using elastin-Congo red. No significant differences were observed among MPAO1-19, -20, -21, and -22 ($p = 0.879$). In contrast, both evolved strains MPAO1-23A and MPAO1-23B exhibited a significant 4.57-fold increase in proteolytic activity ($p < 0.001$), indicating a consistent enhancement in elastase function. Notably, no difference in elastase activity was detected between these two MPAO1-M variants ($p = 0.551$). (Fig. 4).

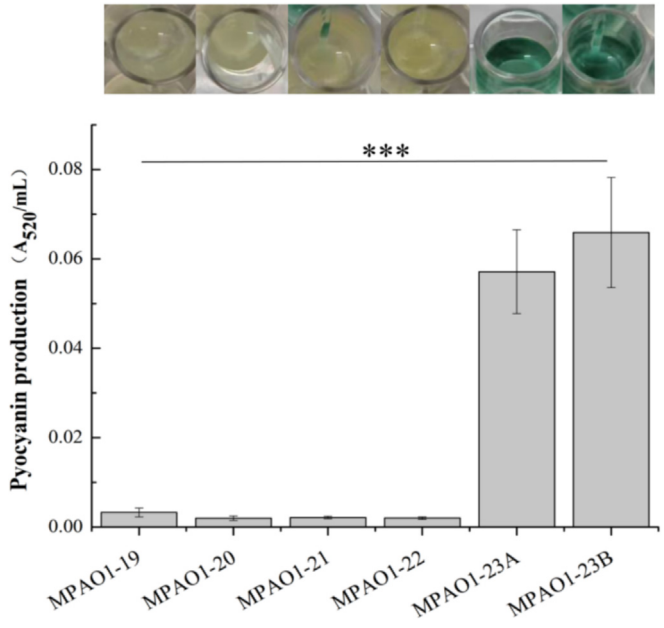

Fig. 2. Pyocyanin production of MPAO1 derivatives. Absorbance measurements were normalized to cell density and calculated as A_{530}/mL. Data represent mean ± SD from the biological replicates ($n = 3$). ***$p < 0.001$.

3.3.4. Motility

The motility of MPAO-19 and its propagated strains was evaluated using Swimming, swarming and twitching assays. Similar swarming and swimming motility levels were observed across the tested strains ($p = 0.07$ for swarming, Fig. 5A; $p = 0.604$ swimming, Fig. 5B). However, twitching assays conducted on 1% LB agar demonstrated that both MPAO1-23A and MPAO1-23B exhibited comparable migration capacities, which were significantly 3.03-fold enhanced compared to the MPAO1-P strains ($p < 0.001$, Fig. 5C).

3.3.5. Biofilm

Biofilm formation capacity among MPAO1 strains was assessed by crystal violet staining, a semi-quantitative method. Following 24-h incubation, assays revealed similar biofilm formation capacity across strains ($p = 0.688$, Fig. 6). After 48 h, the strains MPAO1-23A and -23B displayed a significant 1.35-fold increase ($p < 0.001$) compared to MPAO1-P strains MPAO1-19, -20, -21, and -22, indicating enhanced capability for total biofilm biomass accumulation at 48 h. It should be noted that the crystal violet staining method quantifies bound dye correlating with biofilm biovolume but does not provide insight into the spatial architecture of the biofilm or the metabolic activity/viability of cells within it.

3.4. Genomic basis of phenotypic divergence between MPAO1 sublines

To elucidate the genomic basis underlying phenotypic differences between MPAO1-P and MPAO1-M sublines, WGRS of the MPAO1-P strain (MPAO1-21) and the MPAO1-M subline (MPAO1-23B) was performed. Our analysis demonstrated the absence of copy number variations (CNVs) in both sublines. Notably, both sublines carried an identical SNP in *prpF*, which encodes putatively 2-methylaconitate cis–trans isomerase (Table 6). Beyond this conserved polymorphism, comprehensive genomic comparison revealed distinct variant profiles between the sublines.

Specifically, MPAO1-P type strain MPAO1-21 harbored four variations: two nonsynonymous SNPs, one in MPAO1_01510, encoding a putative EAL domain-containing protein, and another in MPAO1_23995, encoding the type IV fimbrial assembly protein PilB, as well as a frameshift deletion in *pilM*, which encodes the pilus assembly protein PilM, and a nonsense mutation in *fimV*, encoding the motility protein FimV.

In contrast, MPAO1-M type strain carried three missense SNPs located in *mexT* (a transcriptional regulator of the MexEF-OprN efflux pump), *pdxH* (encoding a putative pyridoxamine 5′-phosphate oxidase), and MPAO1_16135 (putatively encoding a prepilin-type cleavage/methylation domain-containing protein), along with a 6-bp insertion in *fhaI*, a gene essential for type VI secretion system (T6SS) assembly, secretion, and hemolytic activity. Notably, the *mexT* SNP results in an alanine-to-valine substitution at residue 30 (A30V). To our knowledge, this represents the first report of a mutation at this residue in *P. aeruginosa.*

3.5. Transcriptional profiling in MPAO1 sublines

The transcriptional regulator MexT governs antibiotic resistance and virulence in *P. aeruginosa* principally by regulating the MexEF-OprN efflux pump, which influences both drug efflux efficiency and QS signaling [20,27]. To delineate the functional consequences of *mexT* mutation in MPAO1-M, we performed qRT-PCR

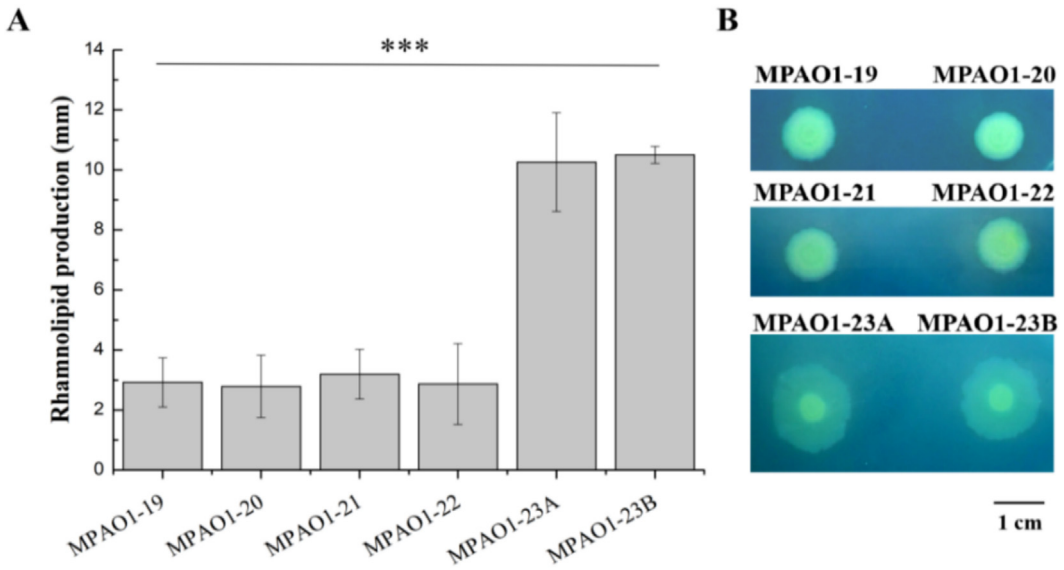

Fig. 3. Rhamnolipid production of MPAO1 strains. (A) Normalized rhamnolipid production was expressed as halo size minus colony size. Data represent mean ± SD from the biological replicates (n = 3) per strain. ***p < 0.001. B: Halos of MPAO1 strains formed on the agar plate.

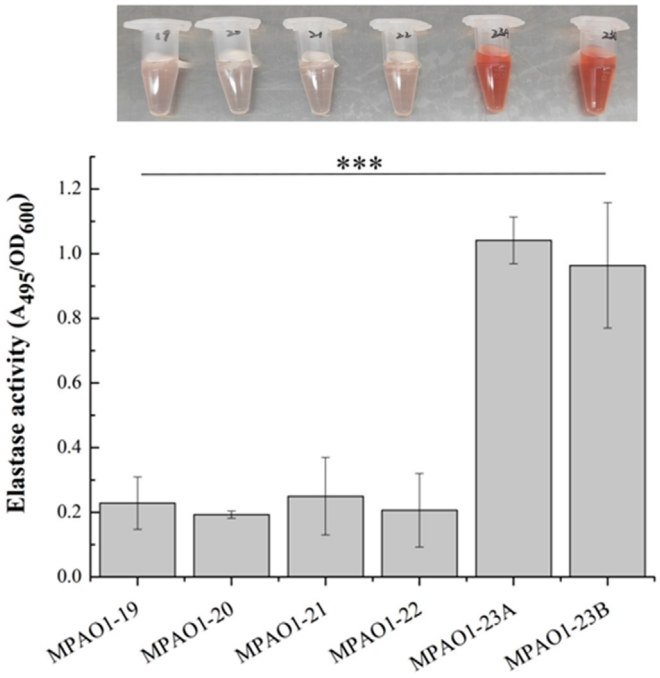

Fig. 4. Elastase activity of MPAO1 strains. Absorbance measurements were normalized to cell density and calculated as A_{495}/OD_{600}. Data represent mean ± SD from the biological replicates (n = 3) per strain. *p < 0.05; **p < 0.01.

analysis of *mexE*, *mexF*, *oprN*, and key QS system genes (*las*, *rhl*, and *pqs* clusters). Our results demonstrated that MPAO1-M exhibited significantly lower transcription levels of *mexE* (90-fold, p < 0.001), *mexF* (56-fold, p < 0.001) and *oprN* (100-fold, p = 0.003) compared to MPAO1-P (Fig. 7A), indicating suppressed expression of the MexEF-OprN efflux pump. Furthermore, among the core genes of the Las, Rhl and PQS systems, MPAO1-M showed significantly elevated expression level of *rhlI* (4.44-fold, p = 0.011) and *pqsA* (4.28-fold, p = 0.001) relative to MPAO1-P (Fig. 7B). These findings suggest a correlation between virulence phenotype differences in the two MPAO1 sublines and their divergent QS system expression patterns, thereby supporting the model in which the *mexT* mutation may lead to decreased MexEF-OprN efflux pump expression and consequently could influence both P. aeruginosa antibiotic resistance and pathogenicity.

4. Discussion

4.1. Phenotypic variations in P. aeruginosa MPAO1 strains

As a globally prevalent nosocomial pathogen, *P. aeruginosa* poses marked clinical challenges owing to its high morbidity and extensive antibiotic resistance [28]. The wild-type *P. aeruginosa* PAO1 strain has been widely utilized as a reference organism in bacterial virulence studies. However, emerging evidence reveals significant genomic and phenotypic divergence among its derivatives. Notably, the MPAO1 strain, a widely used parental line for transposon-insertion mutant libraries, demonstrates distinct genetic variations that translate into altered virulence and resistance profiles compared to PAO1, including decreased antibiotic susceptibility to imipenem, fluoroquinolones, and chloramphenicol [20], as well as attenuated virulence traits, such as reduced twitching motility and pyocyanin production [10]. These differences highlight the phenotypic plasticity of *P. aeruginosa* and the need for strain-specific characterization in pathogenicity and resistance studies.

Consistent with this plasticity, the MPAO1 lineage itself shows notable phenotypic variability. A striking example is the MPAO1-P2 variant described by Olivas et al. [29], which displayed enhanced virulence relative to the parental MPAO1-P1 strain, including elevated pyocyanin production, increased collagenase activity, enhanced swarming motility, and greater tissue-damaging capacity. These traits were linked to mutations in mexT and mexF [26].

In our study, comparative analysis of lab-maintained MPAO1 strains revealed two distinct sublines: MPAO1-P and MPAO1-M. The MPAO1-M subline exhibited elevated virulence, including increased production of pyocyanin, rhamnolipid, and elastase, as well as enhanced twitching motility. Despite its hypervirulence, MPAO1-M showed heightened susceptibility to antimicrobials, a profile consistent with the reported P2 variant [26], except that MPAO1-M retained wild-type swarming motility alongside altered twitching. Notably, MPAO1-M formed more robust biofilms, likely

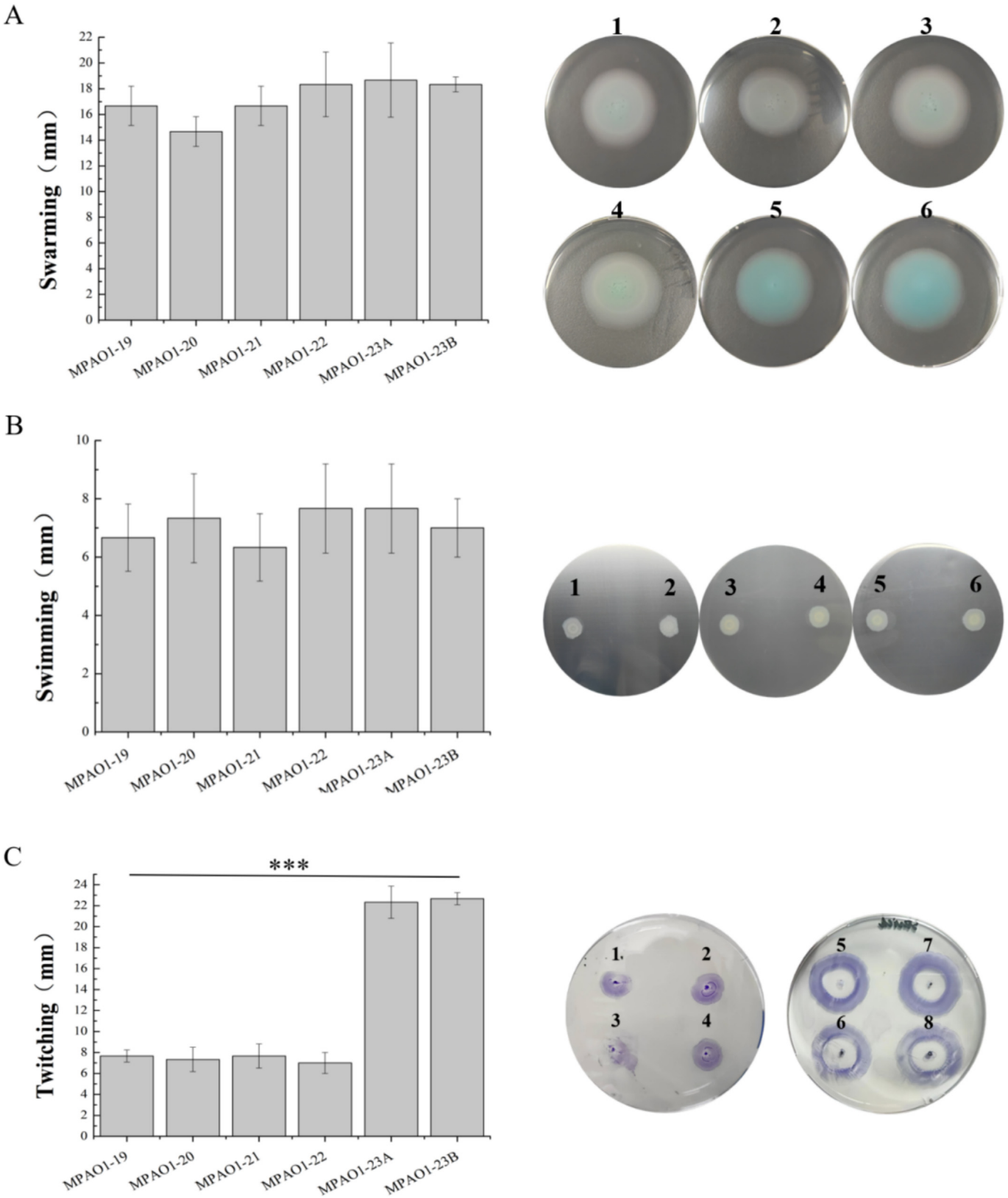

Fig. 5. Motility capacity of MPAO1 strains. (A) Swarming; (B) Swimming; (C) Twitching motility. Data represent mean ± SD from the biological replicates (n = 3) per strain. *** $p < 0.001$. The numbers 1–8 on the plates in each panel correspond to the following strains, separately: 1, MPAO1-19; 2, MPAO1-20; 3, MPAO1-21; 4, MPAO1-22; 5 and 7, MPAO1-23A; 6 and 8, MPAO1-23B.

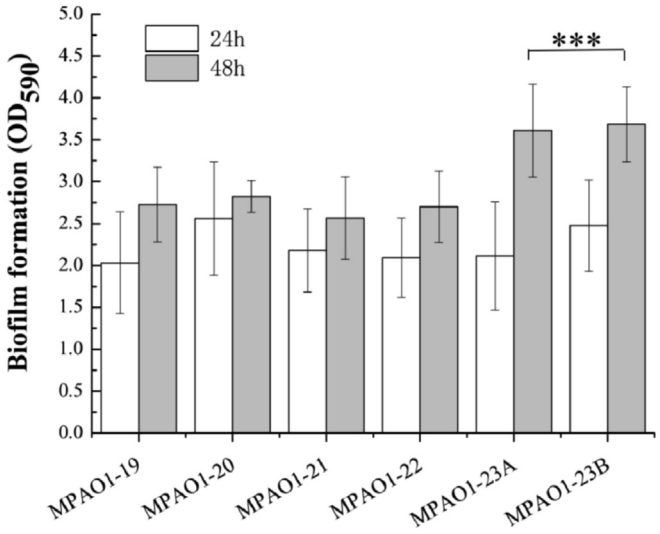

Fig. 6. Biofilm formation of MPAO1 derivatives. Biofilm was quantified by crystal violet staining after 24 h and 48 h incubation. Data represent mean ± SD (n = 6 biological replicates). ***: $p < 0.001$ (MPAO1-23A, 23B group vs. MPAO1-19, 20, 21, 22 group at 48 h). All other comparisons showed no significant differences ($p > 0.05$).

due to higher rhamnolipid production and improved twitching capability. In addition, MPAO1-M showed enhanced susceptibility to chloramphenicol (consistent with P2) and newly identified increased susceptibility to ciprofloxacin, gentamicin, and imipenem. These results broaden the known phenotypic range of MPAO1 sublines and highlight the strain's remarkable phenotypic plasticity.

4.2. What potential factors may contribute to the phenotypic variations in MPAO1?

WGRS demonstrated a high degree of genomic identity between the MPAO1-M and MPAO1-P strains. Both shared a common SNP in *prpF*, which encodes a metabolic enzyme involved in the 2-methylcitrate cycle [30]. However, the in vivo function of PrpF in P. aeruginosa remains experimentally uncharacterized. Although metabolic adaptations can indirectly influence bacterial fitness, this observation aligns with the absence of direct evidence connecting PrpF to canonical antibiotic resistance or virulence pathways.

MPAO1-P was found to harbor specific mutations in four genes, all potentially implicated in bacterial motility. These consist of a frameshift deletion (652delA) in pilM, two SNPs in pilB (G815T) and MPAO1-01510 (G1234A), as well as a nonsense mutation in

Table 6
List of SNPs and InDels in MPAO1 sublines.

Category	Position	Locus tag	Gene	REF	ALT	Mutation type	Encoded product
MPAO1-M/MPAO1-P	4,645,232	MPAO1_22030	*prpF*	C	A	Nonsynonymous SNP	2-methylaconitate cis–trans isomerase PrpF
MPAO1-M(s)	2,707,665	MPAO1_13040	*mexT*	G	A	Nonsynonymous SNP	transcriptional regulator MexT
MPAO1-M	3,438,667	MPAO1_16135	*pdxH*	G	C	Nonsynonymous SNP	pyridoxamine 5′-phosphate oxidase PdxH
MPAO1-M	98,419	MPAO1_00450	*f'ha'l*	C	CTGGCTG	Nonframeshift insertion	type VI secretion system-associated FHA domain protein FhaI
MPAO1-M	5,068,903	MPAO1_23990		A	C	Nonsynonymous SNP	prepilin-type cleavage/methylation domain-containing protein
MPAO1-P	5,690,642	MPAO1_26855	*pilM*	GT	G	frameshift deletion	pilus assembly protein PilM
MPAO1-P	318,878	MPAO1_01510		C	T	nonsynonymous SNP	EAL domain-containing protein
MPAO1-P	5,070,094	MPAO1_23995	*pilB*	G	T	nonsynonymous SNP	type IV fimbrial assembly protein PilB
MPAO1-P	2,017,879	MPAO1_09665	*fimV*	C	T	Nonsense SNP	motility protein FimV

(s): Sanger sequencing confirmed.

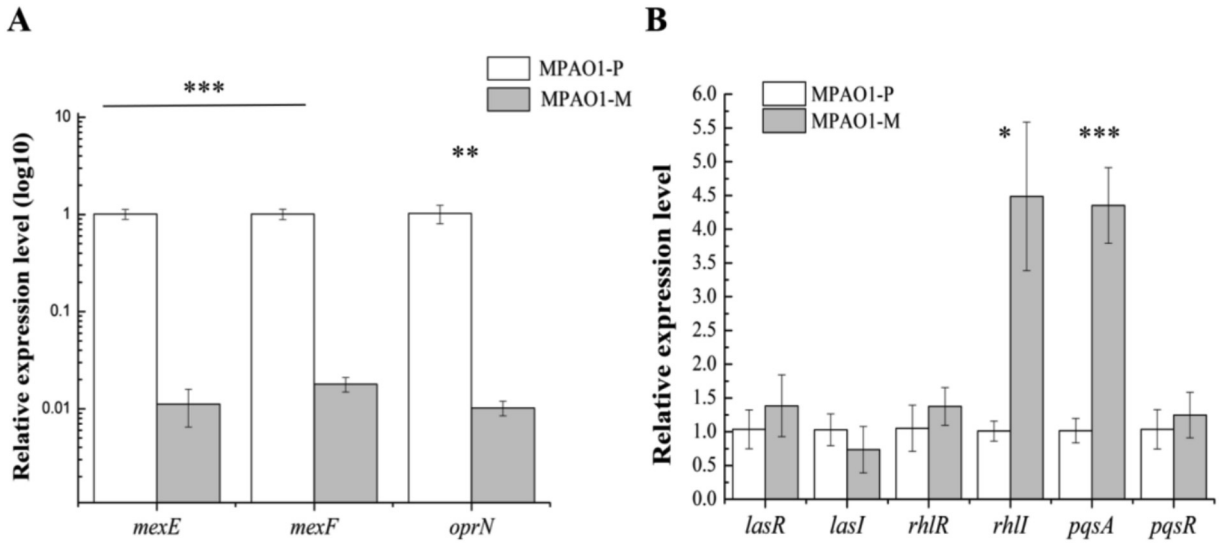

Fig. 7. Transcription level of phenotype-associated regulatory genes in MPAO1 sublines. (A) Genes of MexEF/OprN efflux pump; (B) Essential genes of QS systems. Data represent mean ± SD from the biological replicates (n = 3), $^{*}p < 0.05$, $^{***}p \leq 0.001$.

fimV (C736T). Both *pilM* and *pilB* encode essential components of the Type IV Pilus (T4P) system: PilM is part of a structural complex that anchors the T4P machinery, while PilB acts as an ATPase that powers pilus extension. Mutations in these genes are likely to impair T4P-dependent functions such as twitching motility and adhesion [31]. Additionally, fimV is known to modulate twitching motility in type IVa pilus systems via regulation of cyclic AMP (cAMP) levels [32]. The identified nonsense mutation is likely to result in a truncated, non-functional protein, thereby compromising cAMP-mediated signaling and T4P activity.

Furthermore, the SNP in MPAO1_01510 introduced a missense mutation (D412N) within a putative EAL domain-containing protein. EAL domain proteins are widespread in bacteria and often associated with GGDEF motifs involved in c-di-GMP synthesis [33]. These proteins are implicated in regulating virulence-related behaviors, including motility and biofilm formation [34,35]. The identified SNP is predicted to lie within the GGDEF motif, suggesting a potential impact on c-di-GMP signaling. As c-di-GMP levels positively correlate with biofilm formation but negatively with motility, MPAO1_01510 represents a plausible candidate to explain the concurrent reductions observed in MPAO1-P's twitching motility and biofilm formation at 48 h. However, the simultaneous inhibition of both behaviors contradicts the established paradigm of c-di-GMP signaling. Therefore, the functional consequences of this mutation, as well as its mechanism of action, require further experimental investigation.

The MPAO1-M strain carried 4 specific variations. Among these, two SNPs were located in MPAO1_16135 and MPAO1_23990. MPAO1_16135 is annotated as a putative pyridoxamine 5′-phosphate oxidase *pdxH* that is involved in the pyridoxal 5′-phosphate (PLP) salvage pathway [36]. Although PLP biosynthesis is essential for the survival and virulence of Mycobacterium tuberculosis, the function of its putative homolog *pdxH* in P. aeruginosa remains unknown.

MPAO1_23990 is predicted to encode a prepilin-type protein containing a cleavage/methylation domain. SMART-BLAST analysis indicated that it shares a conserved domain with PilA from Neisseria meningitidis (Query cover: 39%; Identity: 61.02%; E-value: 5e-14). PilA acts as a response regulator in a two-component system and modulates meningococcal adhesiveness [37].

Additionally, a 6-bp insertion was identified in MPAO1_16135, which encodes FhaI, a critical scaffolding protein that nucleates assembly of the T6SS inner membrane complex and baseplate, thereby initiating T6SS biogenesis [38]. In our study, the specific mutations identified in MPAO1-M have not been previously linked, to our knowledge, to the changes in virulence factor production or antibiotic resistance profiles that we observed. This suggests that these particular genetic changes may represent novel mechanisms or context-dependent modifiers worthy of further investigation.

4.3. Is mexT a potential contributor to the observed phenotypic variations?

Beyond the variations noted above, the MPAO1-M subline carries a SNP in the *mexT* gene, a finding of particular interest, as mutations in this gene are well-established drivers of microevolution in PAO1 laboratory strains [17]. MexT, a LysR-family transcriptional regulator, is known to simultaneously modulate antibiotic resistance (via MexEF-OprN efflux pump regulation) and pathogenicity (through the regulation of multiple virulence factors) [27,39]. The observed downregulation of MexEF-OprN efflux system, which exports multiple antibiotics, including fluoroquinolones and chloramphenicol [13], likely explains the increased susceptibility of MPAO1-M to these antimicrobials, as determined in our study. In contrast, the retained susceptibility to aztreonam in our assays suggests it may not be efficiently extruded by this efflux pump system. However, direct efflux assays would be required to confirm this hypothesis. Additionally, this efflux system suppresses the QS system by expelling signaling molecules, thereby reducing virulence factor expression [40]. The expression profile of MPAO1-M, marked by significant downregulation of mexEF-oprN and concurrent upregulation of rhlI and pqsA, supports the hypothesis that this subline has transitioned from the typical "P1-like" state of MPAO1 to a "P2-like" state [29]. Collectively, we propose that a loss-of-function mutation in mexT mechanistically links the observed phenotypic changes: (1) repression of MexEF-OprN efflux system leads to increased susceptibility to its substrates; (2) concomitant dysregulation of QS results in autoinducer accumulation, upregulation of *rhlI* and *pqsA*, and consequently enhanced production of virulence factors.

Genomic analyses of PAO1 sublines reveal that MexT inactivation can occur through diverse genetic alterations. To our knowledge, the SNP in *mexT* (A30V) identified in MPAO1-M subline represents the first documented instance of this mutation. This laboratory-acquired variant likely emerged under extended in vitro subculturing, repeated freeze–thaw cycles, or chronic

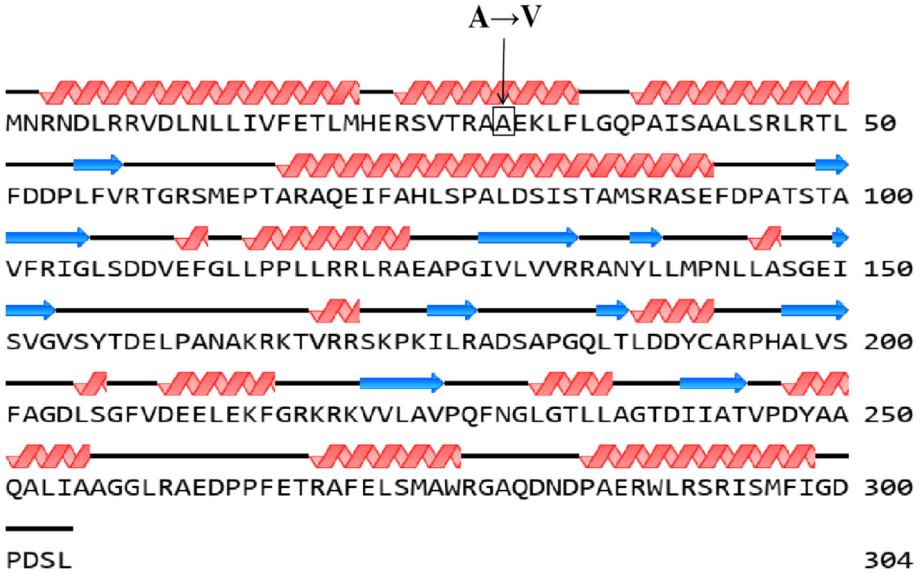

Fig. 8. Secondary structure prediction of MexT in MPAO1-M.

exposure to subinhibitory antibiotic pressures. The A30V substitution localizes within MexT's DNA-binding domain, which exhibits high evolutionary conservation and contains a characteristic helix-turn-helix (HTH) motif. Secondary structure prediction using PSIPRED revealed that the substituted residue resides within the α-helical region of the HTH structure (Fig. 8). We hypothesize that the A30V substitution may compromise the structural integrity of the HTH motif. This could potentially impair its DNA-binding affinity and thereby disrupt its transcriptional regulation function, although future studies, such as electrophoretic mobility shift assays (EMSAs), are needed to validate this model.

Although direct functional validation through genetic complementation remains a goal for future studies, our data provide compelling evidence for its functional impact. Specifically, qRT-PCR analysis revealed a definitive molecular signature of MexT dysregulation: significant downregulation of the *mexEF-oprN* efflux pump operon. Given that MexT is a known transcriptional activator of *mexEF-oprN* operon [29,39], this profound repression provides direct genetic evidence that the A30V substitution impairs MexT function, coherently explaining the observed antibiotic hypersusceptibility. Furthermore, the concomitant upregulation of key QS genes (*rhlI* and *pqsA*) and their effector virulence factors reinforces the link between the *mexT* mutation and enhanced virulence production. Together, these congruent expression changes across MexT's direct and indirect regulatory targets establish a robust causal bridge between the *mexT* A30V genotype and the observed phenotypic divergence.

4.4. Implications for laboratory practice and strain stewardship

Our study provides a stark reminder of the genetic fragility of even well-established model organisms like P. aeruginosa PAO1. The spontaneous emergence of the mexT A30V variant under standard laboratory conditions and its profound effects on core phenotypes of antibiotic resistance and virulence underscore a critical challenge to data reproducibility and cross-study comparisons. This case demonstrates that high-frequency mutational hotspots, such as mexT, can act as genetic traps that ensnare unsuspecting researchers. Therefore, we advocate for the implementation of routine genomic quality control for bacterial strains, particularly those used in long-term projects or those serving as genetic backgrounds for mutant libraries. The integrated phenotypic-genomic-transcriptional framework we employed offers a robust template for diagnosing similar cases of unexplained phenotypic drift. Ultimately, vigilant strain management is not merely a technical formality but a fundamental prerequisite for rigorous and reproducible microbiological research.

CRediT authorship contribution statement

Lingli Zhang: Writing – original draft, Methodology, Conceptualization. **Huiping Qiu:** Writing – review & editing, Methodology. **Shuihong Yao:** Validation. **Pengxia Song:** Data curation. **Zhenghui Li:** Writing – review & editing.

Financial support

This work was supported by Scientific Research Fund of Zhejiang Provincial Education Department (Grant No. Y202147896) and Quzhou Science and Technology Attack Plan Project (Grant No. 2022K107).

Data availability

Data will be made available on request.

Declaration of competing interest

The authors declare no conflict of interest.

Supplementary material

Supplementary data to this article can be found online at https://doi.org/10.1016/j.ejbt.2026.100708.

References

[1] Shao X, Xie Y, Zhang Y, et al. Novel therapeutic strategies for treating *Pseudomonas aeruginosa* infection. Expert Opin Drug Dis 2020;15 (12):1403–23. https://doi.org/10.1080/17460441.2020.1803274. PMid: 32880507.
[2] Abdelaziz AA, Kamer AMA, Al-Monofy KB, et al. *Pseudomonas aeruginosa*'s greenish-blue pigment pyocyanin: Its production and biological activities. Microb Cell Fact 2023;22(1):110. https://doi.org/10.1186/s12934-023-02122-1. PMid: 37291560.
[3] Jurado-Martín I, Sainz-Mejías M, McClean S. *Pseudomonas aeruginosa*: An audacious pathogen with an adaptable arsenal of virulence factors. Int J Mol Sci 2021;22(6):3128. https://doi.org/10.3390/ijms22063128. PMid: 33803907.
[4] Khan F, Pham DTN, Oloketuyi SF, et al. Regulation and controlling the motility properties of *Pseudomonas aeruginosa*. Appl Microbiol Biotechnol 2020;104 (1):33–49. https://doi.org/10.1007/s00253-019-10201-w. PMid: 31768614.
[5] Ramesh R, Rekha ND, Gopal S. *Pseudomonas aeruginosa* biofilm: Treatment strategies to combat infection. Arch Microbiol. 2025;207(6):141. https://doi.org/10.1007/s00203-025-04346-8. PMid: 40348909.
[6] Nickzad A, Déziel E. The involvement of rhamnolipids in microbial cell adhesion and biofilm development - an approach for control? Lett Appl Microbiol 2014;58(5):447–53. https://doi.org/10.1111/lam.12211. PMid: 24372465.
[7] Miranda SW, Asfahl KL, Dandekar AA. *Pseudomonas aeruginosa* quorum sensing. In: Filloux A, Ramos JL, editors. *Pseudomonas aeruginosa*. Adv Exp Med Biol. Cham: Springer; 2022. p. 95–115. https://doi.org/10.1007/978-3-031-08491-1_4. PMid: 36258070.
[8] Vadakkan K, Ngangbam AK, Sathishkumar K, et al. A review of chemical signaling pathways in the quorum sensing circuit of *Pseudomonas aeruginosa*. Int J Biol Macromol 2024;254(Pt 2):127861. https://doi.org/10.1016/j.ijbiomac.2023.127861. PMid: 37939761.
[9] Raya J, Montagut EJ, Marco MP. Analysing the integrated quorum sensing system its potential role in Pseudomonas aeruginosa pathogenesis. Front Cell Infect Microbiol 2025;15:1575421. https://doi.org/10.3389/fcimb.2025.1575421. PMid: 40438239.
[10] Lee J, Zhang L. The hierarchy quorum sensing network in *Pseudomonas aeruginosa*. Protein Cell 2015;6(1):26–41. https://doi.org/10.1007/s13238-014-0100-x. PMid: 25249263.
[11] Pang Z, Raudonis R, Glick BR, et al. Antibiotic resistance in *Pseudomonas aeruginosa*: Mechanisms and alternative therapeutic strategies. Biotechnol Adv 2019;37(1):177–92. https://doi.org/10.1016/j.biotechadv.2018.11.013. PMid: 30500353.
[12] Reynolds D, Kollef M. The epidemiology and pathogenesis and treatment of *Pseudomonas aeruginosa* infections: An update. Drugs 2021;81(18):2117–31. https://doi.org/10.1007/s40265-021-01635-6. PMid: 34743315.
[13] Lorusso AB, Carrara JA, Barroso CDN, et al. Role of efflux pumps on antimicrobial resistance in *Pseudomonas aeruginosa*. Int J Mol Sci 2022;23 (24):15779. https://doi.org/10.3390/ijms232415779. PMid: 36555423.
[14] Braz VS, Furlan JPR, Fernandes AFT, et al. Mutations in NalC induce MexAB-OprM overexpression resulting in high level of aztreonam resistance in environmental isolates of *Pseudomonas aeruginosa*. FEMS Microbiol Lett 2016;363(16):fnw166. https://doi.org/10.1093/femsle/fnw166. PMid: 27412168.
[15] Pan YP, Xu YH, Wang ZX, et al. Overexpression of MexAB-OprM efflux pump in carbapenem-resistant *Pseudomonas aeruginosa*. Arch Microbiol 2016;198 (6):565–71. https://doi.org/10.1007/s00203-016-1215-7. PMid: 27060003.
[16] Suresh M, Nithya N, Jayasree PR, et al. Mutational analyses of regulatory genes, *mexR, nalC, nalD* and *mexZ* of *mexAB-oprM* and *mexXY* operons, in efflux pump hyperexpressing multidrug-resistant clinical isolates of *Pseudomonas aeruginosa*. World J Microbiol Biotechnol 2018;34(6):83. https://doi.org/10.1007/s11274-018-2465-0. PMid: 29846800.
[17] Juarez P, Broutin I, Bordi C, et al. Constitutive activation of MexT by amino acid substitutions results in MexEF-OprN overproduction in clinical isolates of *Pseudomonas aeruginosa*. Antimicrob Agents Chemother 2018;62(5): e02445–e2517. https://doi.org/10.1128/AAC.02445-17. PMid: 29530852.
[18] Chandler CE, Horspool AM, Hill PJ, et al. Genomic and phenotypic diversity among ten laboratory isolates of *Pseudomonas aeruginosa* PAO1. J Bacteriol 2019;201(5):e00595–e618. https://doi.org/10.1128/JB.00595-18. PMid: 30530517.
[19] Klockgether J, Munder A, Neugebauer J, et al. Genome diversity of *Pseudomonas aeruginosa* PAO1 laboratory strains. J Bacteriol 2010;192(4):1113–21. https://doi.org/10.1128/JB.01515-09. PMid: 20023018.

[20] Sidorenko J, Jatsenko T, Kivisaar M. Ongoing evolution of *Pseudomonas aeruginosa* PAO1 sublines complicates studies of DNA damage repair and tolerance. Mutat Res 2017;797–799:26–37. https://doi.org/10.1016/j.mrfmmm.2017.03.005. PMid: 28340408.
[21] Liu Y, Ahator SD, Wang H, et al. Microevolution of the *mexT* and *lasR* reinforces the bias of quorum sensing system in laboratory strains of *Pseudomonas aeruginosa* PAO1. Front Microbiol 2022;13:821895. https://doi.org/10.3389/fmicb.2022.821895. PMid: 35495693.
[22] Clinical and Laboratory Standards Institute (CLSI). Performance Standards for Antimicrobial Susceptibility Testing; 26th Informational Supplement. CLSI document M100-26. Wayne, PA: Clinical and Laboratory Standards Institute; 2016.
[23] Ji PC, Yin KY, Jiang Y, et al. Sesamol: A novel quorum sensing inhibitor and colistin accelerator against *Pseudomonas aeruginosa*. Food Sci Hum Wellness 2024;14(3):1158–68. https://doi.org/10.26599/FSHW.2024.9250075.
[24] Terzi HA, Kulah C, Ciftci IH. The effects of active efflux pumps on antibiotic resistance in *Pseudomonas aeruginosa*. World J Microbiol Biotechnol 2014;30(10):2681–7. https://doi.org/10.1007/s11274-014-1692-2. PMid: 24964907.
[25] Horna G, López M, Guerra H, et al. Interplay between MexAB-OprM and MexEF-OprN in clinical isolates of *Pseudomonas aeruginosa*. Sci Rep 2018;8:16463. https://doi.org/10.1038/s41598-018-34694-z. PMid: 30405166.
[26] Luong PM, Shogan BD, Zaborin A, et al. Emergence of the P2 phenotype in *Pseudomonas aeruginosa* PAO1 strains involves various mutations in *mexT* or *mexF*. J Bacteriol 2014;196(2):504–13. https://doi.org/10.1128/JB.01050-13. PMid: 24244000.
[27] Maseda H, Saito K, Nakajima A, et al. Variation of the *mexT* gene, a regulator of the MexEF-OprN efflux pump expression in wild-type strains of *Pseudomonas aeruginosa*. FEMS Microbiol Lett 2000;192(1):107–12. https://doi.org/10.1111/j.1574-6968.2000.tb09367.x. PMid: 11040437.
[28] De Oliveira DMP, Forde BM, Kidd TJ, et al. Antimicrobial resistance in ESKAPE Pathogens. Clin Microbiol Rev 2020;33(3):e00181–e219. https://doi.org/10.1128/CMR.00181-19. PMid: 32404435.
[29] Olivas AD, Shogan BD, Valuckaite V, et al. Intestinal tissues induce an SNP mutation in *Pseudomonas aeruginosa* that enhances its virulence: Possible role in anastomotic leak. PLoS One 2012;7(8):e44326. https://doi.org/10.1371/journal.pone.0044326. PMid: 22952955.
[30] Garvey GS, Rocco CJ, Escalante-Semerena JC, et al. The three-dimensional crystal structure of the PrpF protein of *Shewanella oneidensis* complexed with *trans*-aconitate: Insights into its biological function. Protein Sci 2007;16(7):1274–84. https://doi.org/10.1110/ps.072801907. PMid: 17567742.
[31] Chang YW, Rettberg LA, Treuner-Lange A, et al. Architecture of the type IVa pilus machine. Science 2016;351(6278):aad2001. https://doi.org/10.1126/science.aad2001. PMid: 26965631.
[32] Buensuceso RNC, Daniel-Ivad M, Kilmury SLN, et al. Cyclic AMP-independent control of twitching motility in *Pseudomonas aeruginosa*. J Bacteriol 2017;199(16):e00188–e217. https://doi.org/10.1128/JB.00188-17. PMid: 28583947.
[33] Simm R, Morr M, Kader A, et al. GGDEF and EAL domains inversely regulate cyclic di-GMP levels and transition from sessility to motility. Mol Microbiol 2004;53(4):1123–34. https://doi.org/10.1111/j.1365-2958.2004.04206.x. PMid: 15306016.
[34] Ha DG, O'Toole GA. c-di-GMP and its effects on biofilm formation and dispersion: A *Pseudomonas aeruginosa* Review. Microbiol Spectr 2015;3(2):MB-0003-2014. https://doi.org/10.1128/microbiolspec.MB-0003-2014 PMid: 26104694.
[35] Kuchma SL, Delalez NJ, Filkins LM, et al. Cyclic di-GMP-mediated repression of swarming motility by *Pseudomonas aeruginosa* PA14 requires the MotAB stator. J Bacteriol 2015;197(3):420–30. https://doi.org/10.1128/JB.02130-14. PMid: 25349157.
[36] Ankisettypalli K, Cheng JJ, Baker EN, et al. PdxH proteins of mycobacteria are typical members of the classical pyridoxine/pyridoxamine 5'-phosphate oxidase family. FEBS Lett 2016;590(4):453–60. https://doi.org/10.1002/1873-3468.12080. PMid: 26823273.
[37] Taha MK, Giorgini D, Nassif X. The *pilA* regulatory gene modulates the pilus-mediated adhesion of *Neisseria meningitidis* by controlling the transcription of *pilC1*. Mol Microbiol 1996;19(5):1073–84. https://doi.org/10.1046/j.1365-2958.1996.448979.x. PMid: 8830264.
[38] Pei TT, Wang XY, Zhang YQ, et al. Fha initiates the inside-out assembly of the type VI secretion system. Cell Rep 2025;44(7):115990. https://doi.org/10.1016/j.celrep.2025.115990. PMid: 40650907.
[39] Kristensen R, Andersen JB, Rybtke M, et al. Inhibition of *Pseudomonas aeruginosa* quorum sensing by chemical induction of the MexEF-oprN efflux pump. Antimicrob Agents Chemother 2024;68(2):e0138723. https://doi.org/10.1128/aac.01387-23. PMid: 38189278.
[40] Maddocks SE, Oyston PCF. Structure and function of the LysR-type transcriptional regulator (LTTR) family proteins. Microbiology 2008;154(12):3609–23. https://doi.org/10.1099/mic.0.2008/022772-0. PMid: 19047729.